Geophys. J. R. astr. Soc. (1986) **87**, 753–773

Amplitude, phase and path anomalies of mantle waves

J. H. Woodhouse and Y. K. Wong *Department of Earth and Planetary Sciences, Harvard University, Cambridge, MA 02138, USA*

Accepted 1986 May 7. Received 1986 April 30; in original form 1985 August 14

Summary. The amplitude and phase anomalies observed in long period Rayleigh and Love waves ($T > 150$ s) show definite patterns of variation from orbit to orbit. In some cases the phase anomalies agree with the prediction of linear perturbation theory applied to a spherical reference model (Fermat's Principle), namely that each complete orbit of the earth in either direction corresponds to a constant phase anomaly increment. The corresponding approximation for amplitude anomaly is derived in this study; it is shown that orbits of one sense are amplified (or deamplified) by a constant factor for each complete orbit, and that orbits of the opposite sense are amplified (or deamplified) by the reciprocal factor. This amplification is due to partial focusing and defocusing of a ray bundle. The data often show such behaviour, establishing that the large observed anomalies are caused by focusing and defocusing due to heterogeneity. Some of the data, however, show substantial deviations from these approximations, indicating that lateral refraction is sometimes a large effect for high orbits. Evidence is presented for orbits which have paths deviating from the great circle by more than 1000 km. A technique is outlined for making use of such data to constrain lateral variations in earth structure.

Key words: surface waves, amplitudes, mantle waves

Introduction

Many studies have made use of very long period surface waves – or 'mantle waves' – to investigate lateral heterogeneities in the Earth's mantle (e.g. Toksöz & Anderson 1966; Kanamori 1970; Dziewonski 1971; Mills 1978; Dziewonski & Steim 1982; Nakanishi & Anderson 1982, 1983). Although a number of different methodologies have been employed, the technique is essentially to make measurements of phase anomaly over a band of frequencies, and to interpret these in terms of phase integrals along the path. The path may be a minor or a major arc (R_1, R_2, G_1, G_2), or one involving one or more complete great circle orbits (R_3, R_4, G_3 G_4, etc.). Invariably the assumption is made that the theoretical phase anomaly is given by a line integral along the great circle defined by the source and

receiver – i.e. that deviations in the path may be neglected for the purpose of calculating phase. We shall refer to this as the 'path integral approximation'. The validity of the approximation, for sufficiently small heterogeneities in phase velocity, derives from Fermat's principle, which guarantees that for a global phase velocity heterogeneity

$$\delta c(\theta, \phi) = \epsilon c_1(\theta, \phi),$$

the phase anomaly will be given by the phase integral approximation to order ϵ^2, for sufficiently small ϵ.

The recently constructed models of global heterogeneity (Nakanishi & Anderson 1982, 1983; Woodhouse & Dziewonski 1984) enable us to perform exact ray tracing for mantle waves in order to check the validity of Fermat's principle, and to find to what extent paths are expected to deviate from the great circle.

A related problem is that of amplitudes. It has been known for some years (it was first pointed out by H. Kanamori) that mantle waves show large amplitude anomalies. In the period range 150 to 300 s factors of 2 or 3 are common. Fig. 1 shows an observed (top) and a synthetic (bottom) trace containing Rayleigh wave orbits $R_1 - R_6$. In this example it is readily seen that odd orbit groups are considerably smaller than predicted and even orbit groups are larger. It is difficult to explain such anomalies except as the effect of focusing and defocusing by heterogeneity. It is well known that the effects of source finiteness may lead to amplitude anomalies for surface wave groups which leave the source in opposite directions and this could lead to systematically large even orbits and small odd orbits, for example. It will be shown below, however, that the amplitude anomalies increase in a regular way with orbit number – a phenomenon which cannot be explained in terms of source directivity. Attenuation differing from that of the reference earth model used in the synthetic calculations may also lead to systematically small or large arrivals; we shall show, however, that amplitude anomalies are usually of opposite sense for even and odd orbits and thus anomalous attenuation is not a viable explanation. In any case an approximate quantitative evaluation of likely attenuation and source effects would lead us to reject them, since the observed anomalies are so large.

The recently constructed global models of mantle heterogeneity have enabled us to investigate the likely effects of low-order phase velocity variations (Wong & Woodhouse 1983, 1984; Lay & Kanamori 1985). We have concluded that both the character and the magnitude of the observed amplitude effects can be explained by heterogeneity of the type contained in these global models. There is clear evidence, both in the data and in synthetic

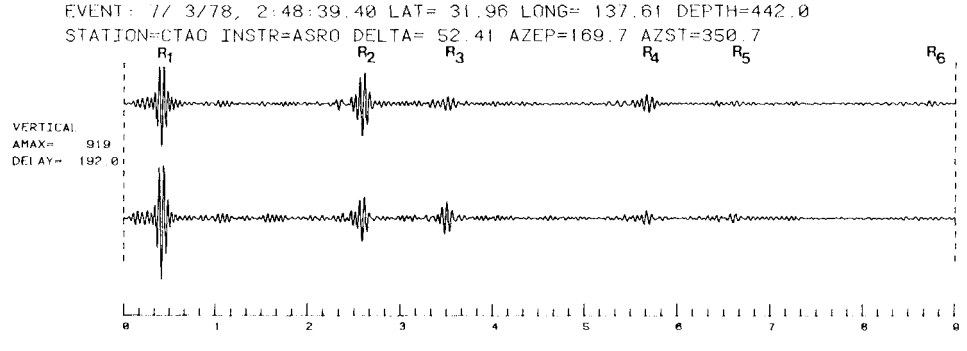

Figure 1. Observed (top) and synthetic (bottom) traces for an event of 1978 March 7 in Japan, observed at Charters Towers, Australia. The record has been low pass filtered, using a cosine taper over the period range 135–155 s.

calculations, of phase anomalies which deviate substantially from the path integral approximation (Fermat's principle). The measure of agreement between theory and observation provides a strong indication that the deviations in path predicted by the models are also realistic. We find that the paths of high orbit Rayleigh and Love waves can deviate from the great circle by as much as 2000 km – even for source–receiver distances close to 90°, for which the great circle path is expected to be most well defined.

It should be noted, however, that the model predictions for amplitudes, and for the departures in phase from Fermat's principle only rarely agree in detail with the observations. These observations constitute, therefore, a valuable new data set which can be used to refine the existing models of heterogeneity.

Our purpose in this paper is to present examples from the data which establish that the general character of the observations is in agreement with that of the model predictions, and to present some theoretical results concerning the way in which observations of this kind are related to the earth's heterogeneity. In particular we derive an approximation to amplitude which is analogous to Fermat's principle for phase, in that it is correct to first order in the heterogeneity and can be calculated in terms of an integral along the unperturbed great circle path. This result shows that, to first order, amplitude anomalies are sensitive to the second derivative of phase velocity transverse to the path, and it is a special case of a more general result which gives the partial derivatives of amplitude and phase anomaly with respect to structural parameter variations, even in the presence of large deviations in path. These could form the basis of an inversion procedure for both amplitude and phase. The fact that successive orbits of mantle waves can sample substantially different paths, and the fact that amplitude anomaly is sensitive to the derivatives of phase velocity, leads us to hope that an analysis based upon a more complete form of ray theory will lead to enhanced resolution of global variations in phase velocity.

Theoretical considerations

THE GENERAL RAY EQUATIONS

For a wave train on a curved surface with slowly varying amplitude and rapidly varying phase, we may approximate the surface displacement field by the first term in the ray series (Woodhouse 1974):

$$u(\mathbf{x}, t) = A(\mathbf{x}, t) \exp [i\psi(\mathbf{x}, t)], \tag{1}$$

where $\mathbf{x} = (x^1, x^2)$ are co-ordinates in the surface and t is time. The covariant components of the local wave vector and the local instantaneous frequency may be defined by:

$$\left.\begin{aligned} k_\sigma &= \frac{\partial \psi}{\partial x_\sigma} \\ \omega &= -\frac{\partial \psi}{\partial t} \end{aligned}\right\} \sigma = 1, 2 \tag{2}$$

and the local dispersion relation $\omega = \omega(\mathbf{k}, \mathbf{x})$ leads to the Hamilton–Jacobi equation for $\psi(\mathbf{x}, t)$ (Woodhouse 1974):

$$\frac{\partial \psi}{\partial t} + \omega\left(\frac{\partial \psi}{\partial x^\sigma}, x^\sigma\right) = 0. \tag{3}$$

The method of characteristics applied to this equation leads to Hamilton's canonical equations:

$$\left.\begin{aligned} \dot{x}^\sigma &= \frac{\partial \omega}{\partial k_\sigma} \\ \dot{k}_\sigma &= -\frac{\partial \omega}{\partial x^\sigma} \end{aligned}\right\} \sigma = 1, 2, \tag{4}$$

where $\cdot$ denotes the total derivative with respect to t along the characteristic curve, or ray. In the terminology of classical mechanics x^σ are generalized coordinates, k_σ are the conjugate momenta and $\omega(k_\sigma, x^\sigma)$ is the Hamiltonian. Since the Hamiltonian has no explicit dependence upon time we also have (e.g. Goldstein 1959)

$$\dot{\omega} = 0. \tag{5}$$

Equations (4) are the ray tracing equations and (5) shows, as we should expect, that the rays correspond to propagation at some fixed frequency. The solutions, $x^\sigma(t)$, represent the trajectory of a wave packet which moves along the ray with the local group velocity:

$$U \equiv \left| \frac{\partial \omega}{\partial k_\sigma} \right| \equiv \left(g_{\sigma\nu} \frac{\partial \omega}{\partial k_\sigma} \frac{\partial \omega}{\partial k_\nu} \right)^{1/2}, \tag{6}$$

where $g_{\sigma\nu}$ is the contravariant metric tensor in the surface; the summation convention is assumed.

These ray equations are valid for any curved surface and for any dispersion relation. In general, the dispersion relation may be azimuthally anisotropic, but here we shall be concerned only with the isotropic case. Defining the wave number

$$k = (g^{\sigma\nu} k_\sigma k_\nu)^{1/2} \tag{7}$$

we assume

$$\omega(k_\sigma, x^\sigma) = \bar{\omega}(k, x^\sigma), \tag{8}$$

where $\bar{\omega}$ is a given function of its arguments. In this case equations (4) become

$$\dot{x}^\sigma = \frac{1}{k} \frac{\partial \bar{\omega}}{\partial k} g^{\sigma\nu} k_\nu \tag{9a}$$

$$\dot{k}_\sigma = -\frac{\partial \bar{\omega}}{\partial x^\sigma} - \frac{1}{2k} \frac{\partial \bar{\omega}}{\partial k} \frac{\partial g^{\alpha\beta}}{\partial x^\sigma} k_\alpha k_\beta. \tag{9b}$$

Since $\bar{\omega}(k, x_\sigma)$ is a constant of the motion, it is convenient to invert the dispersion relation to the form

$$k = k(\omega, x^\sigma). \tag{10}$$

It is easily shown that

$$\left(\frac{\partial \bar{\omega}}{\partial x^\sigma}\right)_k + \left(\frac{\partial k}{\partial x^\sigma}\right)_\omega \left(\frac{\partial \bar{\omega}}{\partial k}\right)_{x^\sigma} = 0, \tag{11}$$

where subscript variables indicate explicitly the quantities held fixed. We shall also define the arc length increment

$$ds = (g_{\sigma\nu}\dot{x}^{\sigma}\dot{x}^{\nu})^{1/2}\,dt = \frac{\partial\bar{\omega}}{\partial k}\,dt, \tag{12}$$

where (9a) has been used. From (11) and (12), equations (9a, b) can be written

$$\left.\begin{aligned} \frac{dx^{\sigma}}{ds} &= \frac{k^{\sigma}}{k} \\ \frac{dk_{\sigma}}{ds} &= \left(\frac{\partial k}{\partial x^{\sigma}}\right)_{\omega} - \frac{1}{2k}\frac{\partial g^{\alpha\beta}}{\partial x^{\sigma}}k_{\alpha}k_{\beta} \end{aligned}\right\}\sigma = 1, 2 \tag{13}$$

where k^{σ} are the contravariant components of the wave vector:

$$k^{\sigma} = g^{\sigma\nu}k_{\nu}.$$

It is interesting to note that the ray equations in the form (13) are independent of group velocity. It may be verified that these are equivalent to the variational problem for $x^{\sigma}(s)$:

$$\delta\int k\,(\omega, x^{\sigma})\,ds = 0 \tag{14}$$

subject to the constraint

$$g_{\sigma\nu}\frac{dx^{\sigma}}{ds}\frac{dx^{\nu}}{ds} = 1. \tag{15}$$

Another useful form of the ray equations may be obtained by deriving Hamilton's equations for the variational problem given by (14). We find that the Hamiltonian is given by:

$$H(k_{\sigma}, x^{\sigma}) = [g^{\alpha\beta}k_{\alpha}k_{\beta}]^{1/2} - k\,(\omega, x^{\sigma}), \tag{16}$$

where x^{σ} are regarded as coordinates and k_{σ} as momenta, and Hamilton's equations:

$$\left.\begin{aligned} \frac{dx^{\sigma}}{ds} &= \frac{\partial H}{\partial k_{\sigma}} \\ \frac{dk_{\sigma}}{ds} &= -\frac{\partial H}{\partial x^{\sigma}} \end{aligned}\right. \tag{17}$$

are then equivalent to (13).

To calculate geometrical spreading we need to consider the equations satisfied by the difference between two neighbouring solutions of the ray equations. Let $[\mathbf{x}(s), \mathbf{k}(s)]$ be a solution of (17), and let $[\mathbf{x}(s) + \mathbf{x}_1(s), \mathbf{k}(s) + \mathbf{k}_1(s)]$ be a second solution, where $\mathbf{x}_1, \mathbf{k}_1$ are small. To first order, $\mathbf{x}_1, \mathbf{k}_1$ satisfy the homogeneous 'bending equations' (Julian & Gubbins 1977), which are obtained by incrementing $\mathbf{x}$ and $\mathbf{k}$ in (17):

$$\left.\begin{aligned} \frac{dx_1^{\sigma}}{ds} &= \frac{\partial^2 H}{\partial k_{\sigma}\partial x^{\nu}}x_1^{\nu} + \frac{\partial^2 H}{\partial k_{\sigma}\partial k_{\nu}}k_{1\nu} \\ \frac{dk_{1\sigma}}{ds} &= -\frac{\partial^2 H}{\partial x^{\sigma}\partial x^{\nu}}x_1^{\nu} - \frac{\partial^2 H}{\partial x^{\sigma}\partial k_{\nu}}k_{1\nu}. \end{aligned}\right. \tag{18}$$

These constitute a linear system for $\mathbf{x}_1, \mathbf{k}_1$, with coefficients evaluated in terms of the unperturbed ray $[\mathbf{x}(s), \mathbf{k}(s)]$. The particular symmetry displayed by (18) enables us to show that if $[\mathbf{x}_1(s), \mathbf{k}_1(s)]$, $[\mathbf{x}_2(s), \mathbf{k}_2(s)]$ are two solutions of (18) then

$$x_1^\sigma k_{2\sigma} - x_2^\sigma k_{1\sigma} = \text{constant}. \tag{19}$$

This follows directly if we make use of (18) to evaluate $d(\mathbf{x}_1 \cdot \mathbf{k}_2 - \mathbf{x}_2 \cdot \mathbf{k}_1)/ds$.

To quantify geometrical spreading we consider a pencil of rays emanating from a point P_1, subtending an angle $d\alpha_1$, and spreading over a perpendicular distance $d\sigma_1$ at the receiver P_2 (see Fig. 2a). Then geometrical spreading for this path may be defined as $d\sigma_1/d\alpha_1$. If the two bounding rays are $[\mathbf{x}(s), \mathbf{k}(s)]$ and $[\mathbf{x}(s) + \mathbf{x}_1(s)d\alpha_1, \mathbf{k}(s) + \mathbf{k}_1(s)d\alpha_1]$, then $[\mathbf{x}_1(s), \mathbf{k}_1(s)]$ satisfy (18), subject to the initial conditions

$$\begin{aligned} &\mathbf{x}_1(P_1) = 0 \\ &k_1^{\parallel}(P_1) = 0, \end{aligned} \tag{20}$$

where $k_1^{\parallel}$ is the component of $\mathbf{k}$ parallel to the ray at P_1. The first of (20) expresses the fact that the two rays emanate from the same point, and the second is required in order that, at P_1:

$$|\mathbf{k}| = |\mathbf{k} + \mathbf{k}_1 d\alpha_1|$$

to first order. Equations (18) and (20) determine $[\mathbf{x}_1(s), \mathbf{k}_1(s)]$ to within a multiplying factor, and we obtain:

$$\frac{d\sigma_1}{d\alpha_1} = \frac{|\mathbf{x}_1^\perp(P_2)|}{|k_1(P_1)|} k(P_1), \tag{21}$$

where $\mathbf{x}_1^\perp$ is the component of $\mathbf{x}_1$ perpendicular to the ray at P_2. Similarly, for the reverse ray (Fig. 2b)

$$\frac{d\sigma_2}{d\alpha_2} = \frac{|\mathbf{x}_2^\perp(P_1)|}{|\mathbf{k}_2(P_2)|} k(P_2), \tag{22}$$

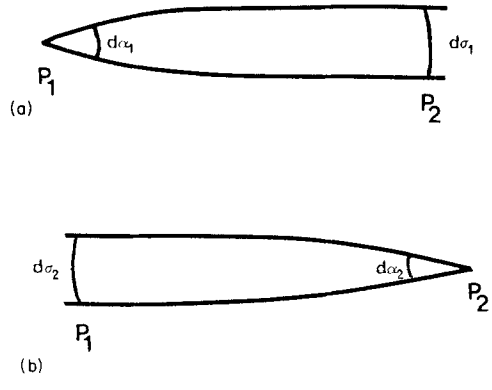

Figure 2. (a) Schematic representation of a pencil of rays emanating from a source at P_1 and travelling to P_2. (b) The reverse path from P_2 to P_1.

where $[\mathbf{x}_2(s), \mathbf{k}_2(s)]$ is the solution of (18) subject to

$$\mathbf{x}_2(P_2) = 0$$
$$\mathbf{k}_2^{\parallel}(P_2) = 0. \tag{23}$$

Since both $(\mathbf{x}_1, \mathbf{k}_1)$ and $(\mathbf{x}_2, \mathbf{k}_2)$ satisfy (18), we may use (19) to write

$$\mathbf{x}_1(P_1) \cdot \mathbf{k}_2(P_1) - \mathbf{x}_2(P_1) \cdot \mathbf{k}_1(P_1) = \mathbf{x}_1(P_2) \cdot \mathbf{k}_2(P_2) - \mathbf{x}_2(P_2) \cdot \mathbf{k}_1(P_2);$$

hence, using the initial conditions (20) and (23)

$$|\mathbf{x}_2^{\perp}(P_1)|\,|\mathbf{k}_1(P_1)| = |\mathbf{x}_1^{\perp}(P_2)|\,|\mathbf{k}_2(P_2)|$$

Thus from (21) and (22) we find

$$\frac{1}{k(P_1)}\frac{d\sigma_1}{d\alpha_1} = \frac{1}{k(P_2)}\frac{d\sigma_2}{d\alpha_2}. \tag{24}$$

This equation expresses the principle of reciprocity for geometrical spreading. A similar result for body waves has been obtained by Richards (1971).

In order to approach the inverse problem we wish to find the perturbation in phase and the perturbation in the spreading factors when the phase velocity model is perturbed: $k(\omega, \mathbf{x}) \to k(\omega, \mathbf{x}) + \delta k(\omega, \mathbf{x})$. The corresponding perturbation in the ray $[\delta\mathbf{x}(s), \delta\mathbf{k}(s)]$ satisfies the inhomogeneous bending equations, which are obtained by perturbing (17):

$$\frac{d}{ds}\delta x^{\sigma} = \frac{\partial^2 H}{\partial k_{\sigma}\partial x^{\nu}}\partial x^{\nu} + \frac{\partial^2 H}{\partial k_{\sigma}\partial k_{\nu}}\partial k_{\nu} + \frac{\partial}{\partial k_{\sigma}}\delta H(k_{\sigma}, x^{\sigma}) \tag{25a}$$

$$\frac{d}{ds}\delta k_{\sigma} = -\frac{\partial^2 H}{\partial x^{\sigma}\partial x^{\nu}}\partial x^{\nu} - \frac{\partial^2 H}{\partial x^{\sigma}\partial k_{\nu}}\delta k_{\nu} - \frac{\partial}{\partial x^{\sigma}}\delta H(k_{\sigma}, x^{\sigma}), \tag{25b}$$

where δH is given by (16)

$$\delta H(k_{\sigma}, x^{\sigma}) = -\delta k(\omega, x^{\sigma}). \tag{26}$$

Note that, in fact, δH is independent of k_{σ} and, thus, the inhomogeneous term in (25a) vanishes. The boundary conditions:

$$\delta\mathbf{x}(P_1) = \delta\mathbf{x}^{\perp}(P_2) = 0$$
$$|\delta\mathbf{k}^{\parallel}(P_1)| = \delta k(P_1), \tag{27}$$

which express the fact that the perturbed ray passes through fixed endpoints and that the dispersion relation is satisfied at the initial point, complete the boundary value problem for $[\delta\mathbf{x}(s), \delta\mathbf{k}(s)]$. Similarly we obtain from (18) the equations for the perturbations in $\mathbf{x}_1(s)$, $\mathbf{k}_1(s)$:

$$\frac{d\delta x_1^{\sigma}}{ds} = \frac{\partial^2 H}{\partial k_{\sigma}\partial x^{\nu}}\delta x_1^{\nu} + \frac{\partial^2 H}{\partial k_{\sigma}\partial k_{\nu}}\delta k_{1\nu} + C^{\sigma}$$
$$\frac{d\delta k_{1\sigma}}{ds} = -\frac{\partial^2 H}{\partial x^{\sigma}\partial x^{\nu}}\delta x_1^{\nu} - \frac{\partial^2 H}{\partial x^{\sigma}\partial k_{\nu}}\partial k_{1\nu} - D_{\sigma}, \tag{28}$$

where the inhomogeneous terms are:

$$C^\sigma = \frac{\partial^3 H}{\partial k_\sigma \partial x^\nu \partial x^\gamma}\,\delta x^\gamma x_1^\nu + \frac{\partial^3 H}{\partial k_\sigma \partial x^\nu \partial k_\gamma}\,\delta k_\gamma x_1^\nu + \frac{\partial^3 H}{\partial k_\sigma \partial k_\nu \partial x^\gamma}\,\delta x^\gamma k_{1\nu}$$
$$+ \frac{\partial^3 H}{\partial k_\sigma \partial k_\nu \partial k_\gamma}\,\delta k_\gamma k_{1\nu} + \frac{\partial^2 \delta H}{\partial k_\sigma \partial x^\nu} x_1^\nu + \frac{\partial^2 \delta H}{\partial k_\sigma \partial k_\nu}\,k_{1\nu};$$

$$D_\sigma = \frac{\partial^3 H}{\partial x^\sigma \partial x^\nu \partial x^\gamma}\,\delta x^\gamma x_1^\nu + \frac{\partial^3 H}{\partial x^\sigma \partial x^\nu \partial k_\gamma}\,\delta k_\gamma x_1^\nu + \frac{\partial^3 H}{\partial x^\sigma \partial k_\nu \partial x^\gamma}\,\delta x^\gamma k_1^\nu$$
$$+ \frac{\partial^3 H}{\partial x^\sigma \partial k_\nu \partial k_\gamma}\,\delta k_\gamma k_1^\nu + \frac{\partial^2 \delta H}{\partial x^\sigma \partial k^\nu} x_1^\nu + \frac{\partial^2 \delta H}{\partial x^\sigma \partial k_\nu}\,k_{1\nu}. \tag{29b}$$

Perturbing (20) the initial conditions are

$$\delta \mathbf{x}_1(P_1) = 0$$
$$\mathbf{k} \cdot \delta \mathbf{k}_1 = -\,\delta \mathbf{k} \cdot \mathbf{k}_1. \tag{30}$$

From (21) we find that the perturbation in the spreading factor is given by:

$$\delta \ln\left(\frac{d\sigma_1}{d\alpha_1}\right) = \frac{1}{k}\,\delta k(P_1) + \frac{1}{|\mathbf{x}_1^\perp(P_2)|^2}\,\mathbf{x}_1^\perp(P_2) \cdot \delta \mathbf{x}_1^\perp(P_2) - \frac{1}{|\mathbf{k}_1(P_1)|^2}\,\mathbf{k}_1(P_1) \cdot \delta \mathbf{k}_1(P_1). \tag{31}$$

This completes the formal steps necessary to find the spreading factors and their perturbations due to structural perturbations. It will be noted that in order to find the derivatives of spreading factors with respect to a large basis set of model perturbations (such as spherical harmonics), it is necessary to solve repeatedly linear systems of equations of the form (25) and (28). These equations are the same, except that they possess different inhomogeneous terms and different boundary conditions. It is natural, and economic, therefore, to use the method of Green's functions; once the Green's function has been tabulated along the unperturbed ray, the calculations reduce to multiple numerical quadratures. The same equations must also be solved in the 'bending' method of ray tracing of Julian & Gubbins (1977). The analagous problem for short period body wave amplitudes has been analysed by Thomson (1983).

RAY THEORY FOR A SPHERE

Here we derive simplified equations for ray tracing and amplitude calculations on a spherical earth. We shall use coordinates $x^1 = \gamma \equiv \cot\theta$ and $x^2 = \phi$, where θ is colatitude and ϕ is longitude. The metric tensor is given by

$$g^{11} = a^{-2}(1+\gamma^2)^2 \qquad g^{12} = 0$$
$$g^{21} = 0 \qquad g^{22} = a^{-2}(1+\gamma^2), \tag{32}$$

where a is earth radius. The ray tracing equations (13) may then be reduced to the following second order differential equation for $\gamma = \gamma(\phi)$:

$$\frac{d^2\gamma}{d\phi^2} + \gamma = \left(\frac{\nu^2}{1+\gamma^2} + 1\right)(\partial_\theta - \nu\partial_\phi) \ln c(\theta, \phi), \tag{33}$$

where $\nu \equiv -d\gamma/d\phi$ and $c = \omega/k$ is phase velocity. Equation (33) is equivalent to the ray tracing equations of Jobert & Jobert (1983). For our current work, the form (33) has the advantage that it is approximately linear in the case of slight heterogeneity. Without loss of generality, we may use a coordinate system in which both the source and the receiver are on the equator, $\gamma = 0$, at longitudes $\phi = 0$ and $\phi = \Delta$, respectively. Equation (33) is then to be solved, subject to the boundary conditions

$$\gamma(0) = \gamma(\Delta) = 0 \tag{34}$$

Equations (33), (34) can readily be solved by the 'shooting' method. Using starting values $\gamma(0) = 0$, $\nu(0) = \nu_0$ (33) may be solved numerically for a given model $\delta c(\theta, \phi)$. It is then necessary to find a value ν_0 such that the boundary condition $\gamma(\Delta) = 0$ is satisfied. If the derivative

$$\frac{\partial}{\partial \nu_0}\gamma(\Delta, \nu_0) \tag{35}$$

is available, Newton's method may be employed; furthermore this derivative is simply related to geometrical spreading. We have, using the notation defined previously,

$$\frac{d\sigma_1}{d\alpha_1} = -a(1+\nu_0^2)\left[1+\nu^2(\Delta)\right]^{-1/2}\frac{\partial}{\partial \nu_0}\gamma(\Delta, \nu_0). \tag{36}$$

Using the notation:

$$\gamma'(\phi) = \frac{\partial}{\partial \nu_0}\gamma(\phi, \nu_0) \tag{37}$$

$$\upsilon'(\phi) = \frac{\partial}{\partial \nu_0}\nu(\phi, \nu_0) = -\frac{\partial}{\partial \phi}\gamma'(\phi, \nu_0)$$

we find, on differentiating (33), (34):

$$\frac{d\gamma'}{d\phi} + \gamma' = \frac{2\nu}{1+\gamma^2}\left(\nu' - \frac{\nu\gamma\gamma'}{1+\gamma^2}\right)(\partial_\theta - \nu\partial_\phi)\ln c - \left(\frac{\nu^2}{1+\gamma^2}+1\right)\frac{\gamma'}{1+\gamma^2}(\partial_\theta^2 - \nu\partial_\theta\partial_\phi)\ln c$$

$$-\left(\frac{\nu^2}{1+\gamma^2}+1\right)\nu'\partial_\phi \ln c \tag{38}$$

$$\gamma'(0) = 0$$

$$\nu'(0) = 1 \tag{39}$$

Equations (38), (39) constitute an initial value problem for $\gamma'(\phi)$ which may be solved numerically, together with (33) to obtain both the ray and $\partial\gamma/\partial\nu_0$. The exact ray tracing experiments to be discussed below were performed using this technique and a Runge–Kutta algorithm.

For a homogeneous earth, $\ln c = \text{const.}$, the solution of (33), (34), (38), (39) is immediate:

$$\gamma(\phi) = 0 \qquad \nu(\phi) = 0$$

$$\gamma'(\phi) = -\sin\phi \qquad \nu'(\phi) = \cos\phi. \tag{40}$$

Equation (36) then leads to

$$\frac{d\sigma_1}{d\alpha_1} = a \sin \Delta$$

which is the familiar result for geometrical spreading on a sphere. In an aspherical earth model, we define amplitude anomaly to be the ratio

$$A = \left| a \sin \Delta \frac{d\alpha_1}{d\sigma_1} \right| = \left| \frac{\sin \Delta}{\gamma'(\Delta)(1+\nu_0^2)} \right|^{1/2} [1+\nu^2(\Delta)]^{1/4}. \tag{41}$$

Thus A is the anomalous amplification due to heterogeneity.

Phase anomaly is defined with respect to a spherically symmetric reference earth model:

$$\delta\psi = \int_{\text{ray}} \frac{\omega}{c(\theta,\phi)} ds - \frac{\omega a}{c_0} \Delta$$

$$= \frac{\omega a}{c_0} \int_0^\Delta \left[\frac{c_0}{c(\theta,\phi)} \left\{ \frac{\nu(\phi)^2}{[1+\gamma^2(\phi)]^2} + \frac{1}{1+\gamma^2(\phi)} \right\}^{1/2} - 1 \right] d\phi, \tag{42}$$

where c_0 is phase velocity in the reference model, and $\theta = \cot^{-1}\gamma(\phi)$.

THE PATH INTEGRAL APPROXIMATION

Before discussing exact ray tracing results for amplitude and phase anomaly, it is of interest to examine their behaviour in the case of slight heterogeneity. The result for phase is well known, and is given by Fermat's principle:

$$\delta\psi = -\frac{\omega a}{c_0} \int_0^\Delta \frac{\delta c(\theta,\phi)}{c_0} d\phi, \tag{43}$$

where the integral is along the great circle $\theta = \pi/2$. Formally this can be obtained by linearizing (42) with respect to $\delta c = c(\theta, \phi) - c_0$. Here we shall find the analogous result for amplification, i.e. we shall seek to linearize (41) with respect to δc. First let us rewrite (33) as an integral equation. The Green's function for the operator $d^2\gamma/d\phi^2 + \gamma$, subject to boundary conditions (34) is

$$G(\phi,\phi') = \begin{cases} -\operatorname{cosec}\Delta \sin\phi \sin(\Delta-\phi') & (\phi < \phi') \\ -\operatorname{cosec}\Delta \sin(\Delta-\phi)\sin\phi' & (\phi > \phi'); \end{cases} \tag{44}$$

i.e. (33) is equivalent to

$$\gamma(\phi) = \int_0^\Delta G(\phi,\phi') f[\gamma(\phi'),\phi'] d\phi', \tag{45}$$

where $f[\gamma, \phi]$ represents the right side of (33). Similarly (38), (39) are equivalent to

$$\gamma'(\phi) = -\sin\phi - \int_0^\phi \sin(\phi-\phi') g[\gamma(\phi'),\gamma'(\phi'),\phi'] d\phi', \tag{46}$$

where $g[\gamma, \gamma', \phi]$ is the right side of (38). If δc is small: $c = 0(\epsilon)$, we have (see equations 40)

$$\gamma(\phi) = 0(\epsilon) \qquad \nu(\phi) = 0(\epsilon)$$
$$\gamma'(\phi) = -\sin\phi + 0(\epsilon) \qquad \nu'(\phi) = \cos\phi + 0(\epsilon) \tag{47}$$

and also

$$\partial_\theta \ln c = 0(\epsilon).$$

Substituting into (33) we find, to first order,

$$\gamma(\phi) \simeq -\int_0^\Delta G(\phi, \phi') c_0^{-1} \partial_\theta \delta c(\pi/2, \phi') d\phi' \tag{48}$$

which is an explicit result for the shape of the perturbed ray. This result can be used to evaluate the initial take-off angle (to first order):

$$\nu_0 = -\left.\frac{d\gamma}{d\phi}\right|_{\phi=0} \simeq \int_0^\Delta \operatorname{cosec}\ \Delta \sin(\Delta - \phi) c_0^{-1} \partial_\theta \delta c(\pi/2, \phi)\, d\phi. \tag{49}$$

This is a useful starting value in the shooting method used for the exact calculations. Similarly the off-azimuth arrival direction is determined by

$$\nu(\Delta) = -\left.\frac{d\gamma}{d\phi}\right|_{\phi=\Delta} \simeq -\int_0^\Delta \operatorname{cosec}\Delta \sin\phi c_0^{-1} \partial_\theta \delta c(\pi, \phi)\, d\phi. \tag{50}$$

It is interesting to note that the deviation from the great circle azimuth is proportional to the path integral of the transverse derivative of phase velocity, multiplied by a kernel $\sin\phi$.

Linearizing equation (46) (see 38, 47) we find

$$\gamma'(\phi) \simeq -\sin\phi + \int_0^\phi \sin(\phi - \phi')[\sin\phi' \partial_\theta^2 - \cos\phi' \partial_{\phi'}] \ln c\, d\phi', \tag{51}$$

where $c = c(\pi/2, \phi')$. Setting $\phi = \Delta$ and substituting into (41) we find that the amplitude anomaly is given by

$$\ln A = \tfrac{1}{2} \operatorname{cosec}\Delta \int_0^\Delta \sin(\Delta - \phi) c_0^{-1} [\sin\phi \partial_\theta^2 - \cos\phi \partial_\phi] \delta c\, d\phi, \tag{52}$$

where $\delta c = \delta c(\pi/2, \phi)$; this is the path integral approximation to amplitude anomaly. Note that amplitude anomaly is principally sensitive to the second transverse derivative of phase velocity with symmetric kernel $\sin(\Delta - \phi)\sin\phi$. For wave propagation in a low velocity trough, $\partial_\theta^2 \delta c > 0$, we obtain amplification, as we might expect.

Let us now consider the behaviour of a phase and amplitude anomaly for multiple orbits of mantle waves. The quantity Δ in the foregoing analysis is simply the value of ϕ at the receiver, $\phi = \phi_r$. For odd orbits R_n, G_n, travelling in the positive ϕ direction, this will be $\phi_r = \Delta + \pi(n-1)$ and for even orbits travelling in the negative direction $\phi_r = \Delta - \pi n$. The linearized formulae (43) and (52) predict systematic behaviour from orbit to orbit, because the integrands are periodic in ϕ. For phase anomaly it is, of course, well known that if Fermat's principle applies the phase anomaly can be written

$$\delta\psi = \begin{cases} -\omega a c_0^{-1}[I_1 + \tfrac{1}{2}(n-1)I_2] & (n \text{ odd}) \\ -\omega a c_0^{-1}[-I_1 + \tfrac{1}{2} n I_2] & (n \text{ even}), \end{cases} \tag{53}$$

where I_1 and I_2 represent the integral in equation (43) taken over the minor arc and the complete great circle, respectively. Thus a plot of phase anomaly against orbit number will produce two parallel lines. From equation (52) we obtain the corresponding result for amplitude anomaly:

$$\ln A = \begin{cases} \tfrac{1}{2}\,\mathrm{cosec}\,\Delta\,[J_1 + \tfrac{1}{2}(n-1)J_2] & (n \text{ odd}) \\ \tfrac{1}{2}\,\mathrm{cosec}\,\Delta\,[J_1 - \tfrac{1}{2}nJ_2] & (n \text{ even}) \end{cases}, \tag{54}$$

where J_1 and J_2 denote the integral in (52) over the minor arc and over the complete great circle. It will be noted that a plot of amplitude anomaly against orbit number should show *opposite* slopes for even and odd orbits, in this approximation. Similarly, from (50), it can be shown that the deviation in azimuth for successive orbits at a given station will be given by

$$\nu = \begin{cases} -K_1 - \tfrac{1}{2}(n-1)K_2 & (n \text{ even}) \\ -K_1 + \tfrac{1}{2}nK_2 & (n \text{ odd}) \end{cases}, \tag{55}$$

where K_1, K_2 are obtained from the integral in (50). Thus, in this approximation, azimuth deviation will accumulate linearily from orbit to orbit, but with the opposite sense for even and odd orbits. Even though this result is only a first approximation, it has rather far-reaching implications, since it demonstrates that there is a tendency for even and odd orbits to separate and thus to travel along systematically different paths. Each successive even or odd orbit, at some fixed range, moves away from the great circle by a fixed amount, and with opposite sense for even and odd orbits. In exact ray tracing calculations this behaviour is reproduced, but tends to saturate when a path of maximum travel time is encountered; the high orbits then become locked into a low velocity path.

It is interesting to note that, by virtue of the invariance of the kernels with respect to the substitutions $\phi \to \phi + \pi$, $\theta \to \pi - \theta$, corresponding to point reflection through the centre of the Earth, the integrals I_2, J_2, K_2 depend only upon the even order spherical harmonic coefficients of phase velocity; thus the terms in equations (53)–(55) which accumulate from orbit to orbit (and thus can be most accurately measured) are insensitive to odd order structure. That this is true for phase anomaly is well known (Backus 1964); the above results show that in the linear approximation the secular terms in both amplitude anomaly and in azimuth deviation have the same property.

DATA AND SYNTHETIC CALCULATIONS

Here we shall show a number of examples of the systematic variation of amplitude and phase anomalies for multiple mantle wave orbits in the period range 150–300 s. In synthetic calculations we shall assume that amplitude anomaly is governed solely by geometrical spreading. Since, in fact, it is horizontal energy flux which is conserved within a ray tube, there are additional amplitude fluctuations due to the differing surface amplitudes of a surface wave of unit energy flux. This effect will amount to only a few percent, since the variations of phase velocity, group velocity and structural parameters are of this order, and thus its contribution will be small compared with that of geometrical spreading. Moreover, it will contribute the same (multiplicative) anomaly to each orbit at a given station and thus will not affect the relative amplitudes of successive orbits.

Several hundreds of records have been analysed and the trends to be described here are universal. The particular examples we discuss are a selection of those which show substantial

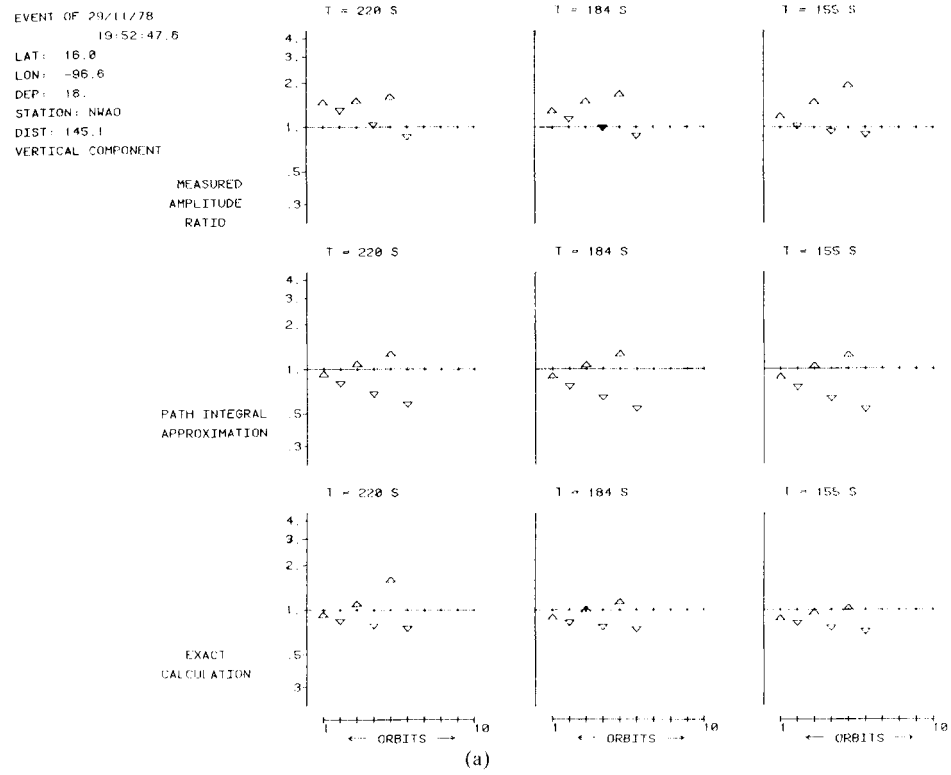

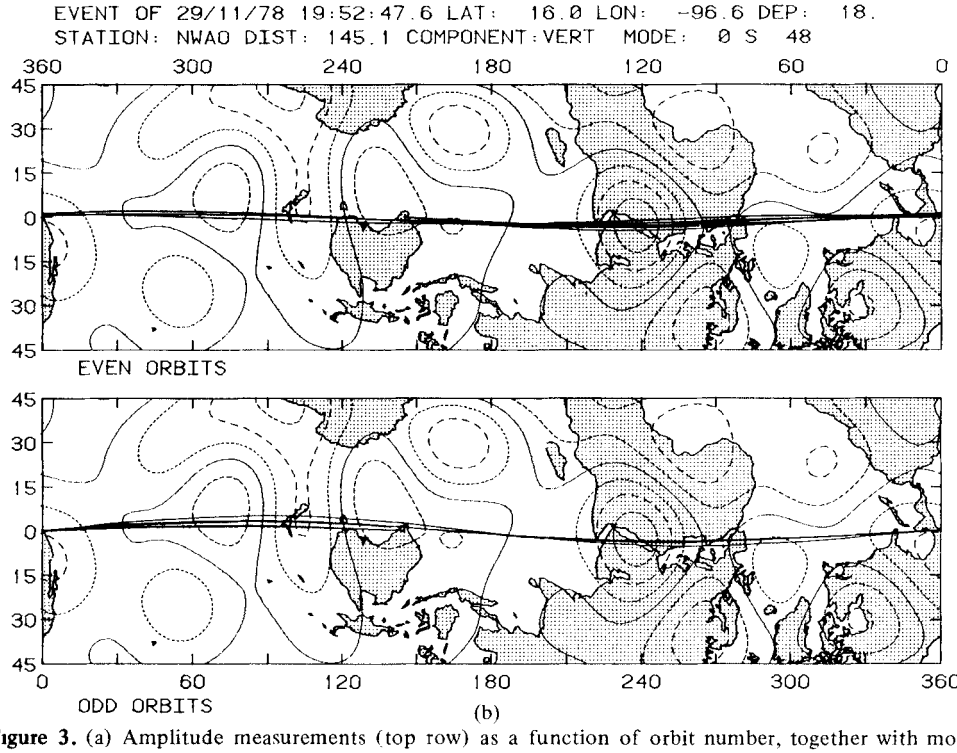

Figure 3. (a) Amplitude measurements (top row) as a function of orbit number, together with model calculations based upon the path integral approximation (middle row) and exact ray tracing (bottom row); the model calculations make use of the model M84C of Woodhouse & Dziewonski (1984). (b) The paths followed by the orbits of Fig. 3(a); all even orbits (top panel) and odd orbits (bottom panel) are superimposed.

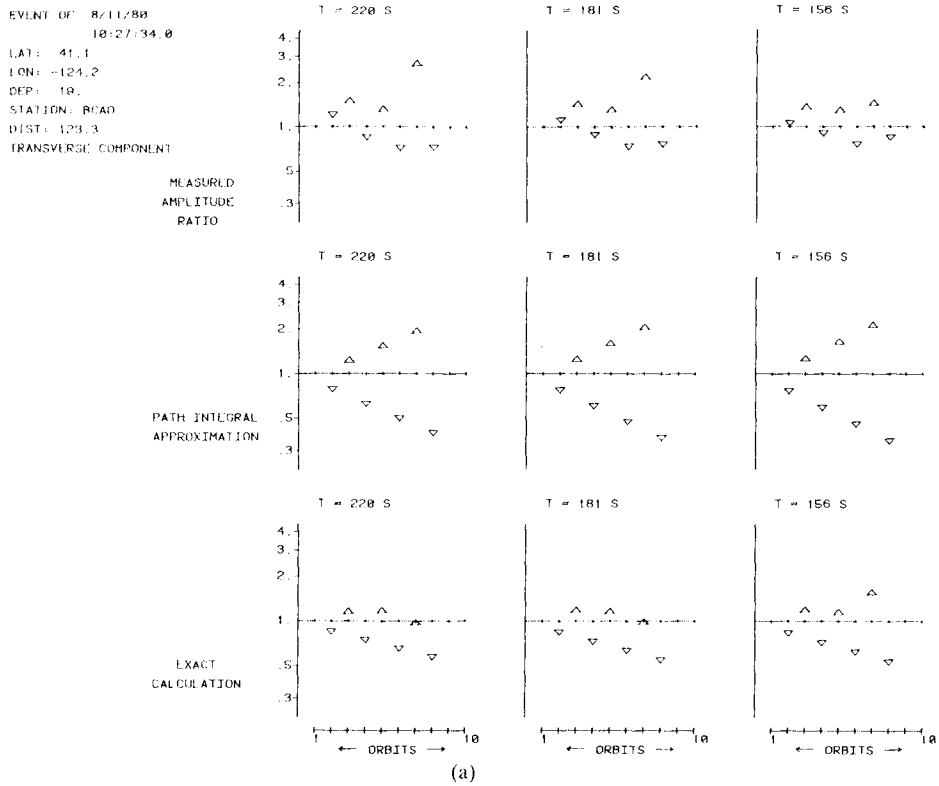

(a)

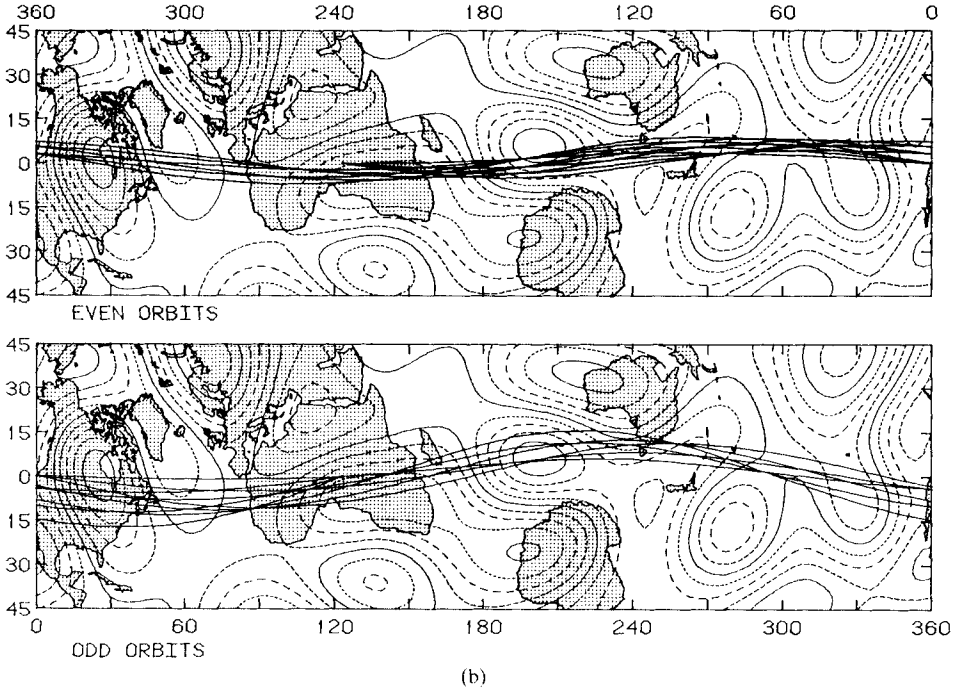

(b)

Figure 4. (a) Amplitude measurements and model calculations. See caption to Fig. 3(a). (b) The paths followed by the orbits of Fig. 4(a).

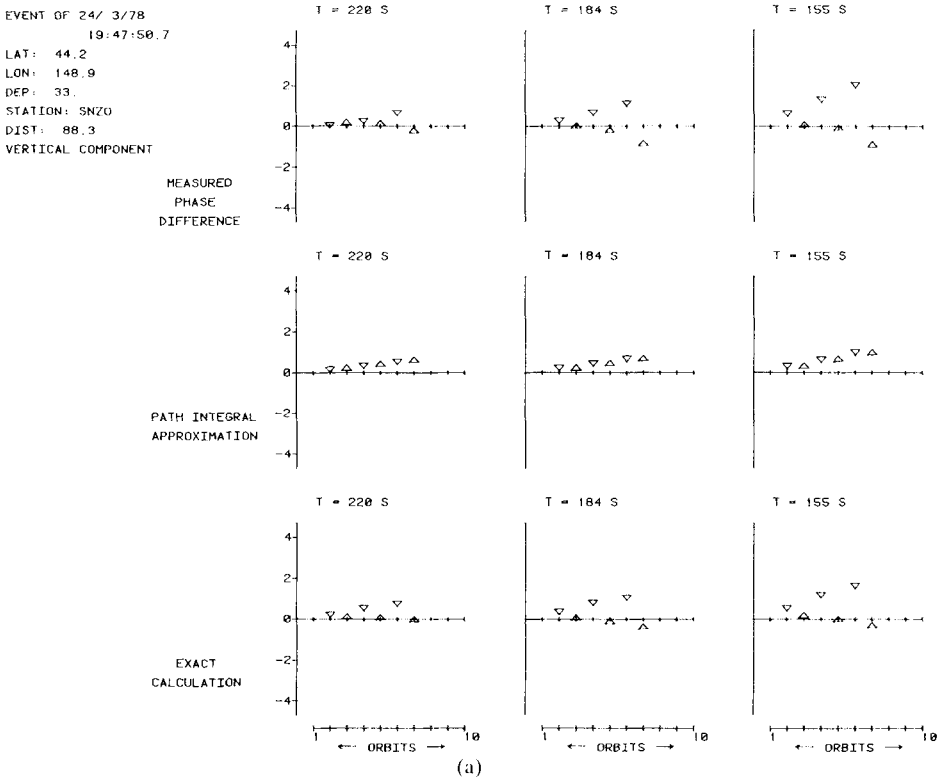

(a)

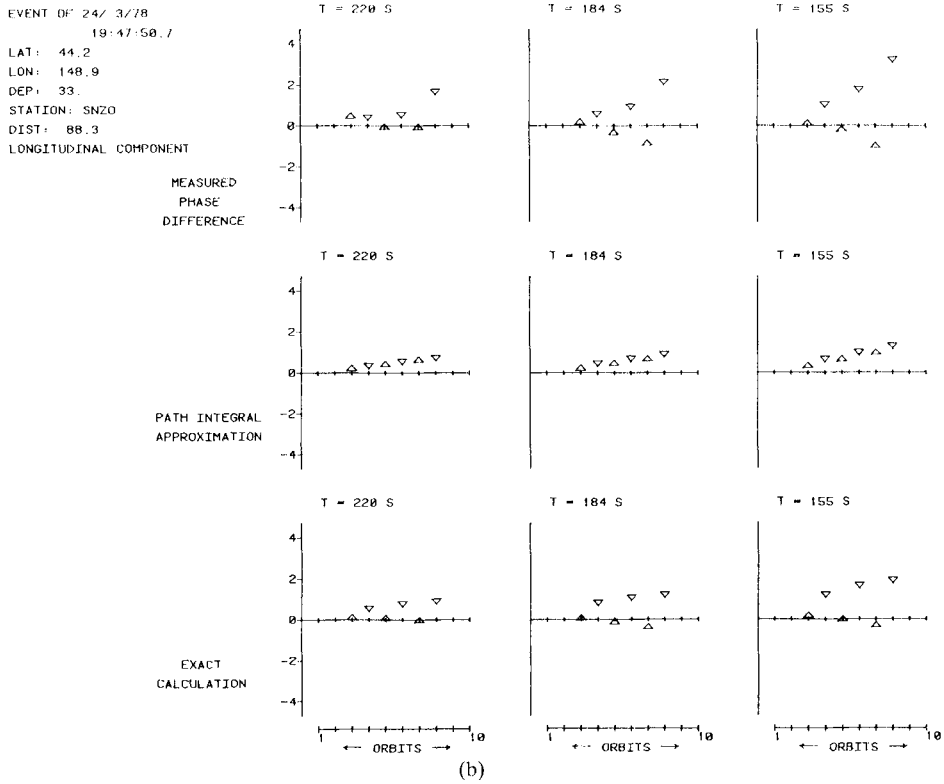

(b)

Figure 5. (a) Phase measurements (top row) as a function of orbit number, together with model calculations based upon Fermat's principle (middle row) and exact ray tracing (bottom row). Vertical component. (b) Same as Fig. 5(a) but for longitudinal component. (c) Paths followed by orbits of Fig. 5(a, b).

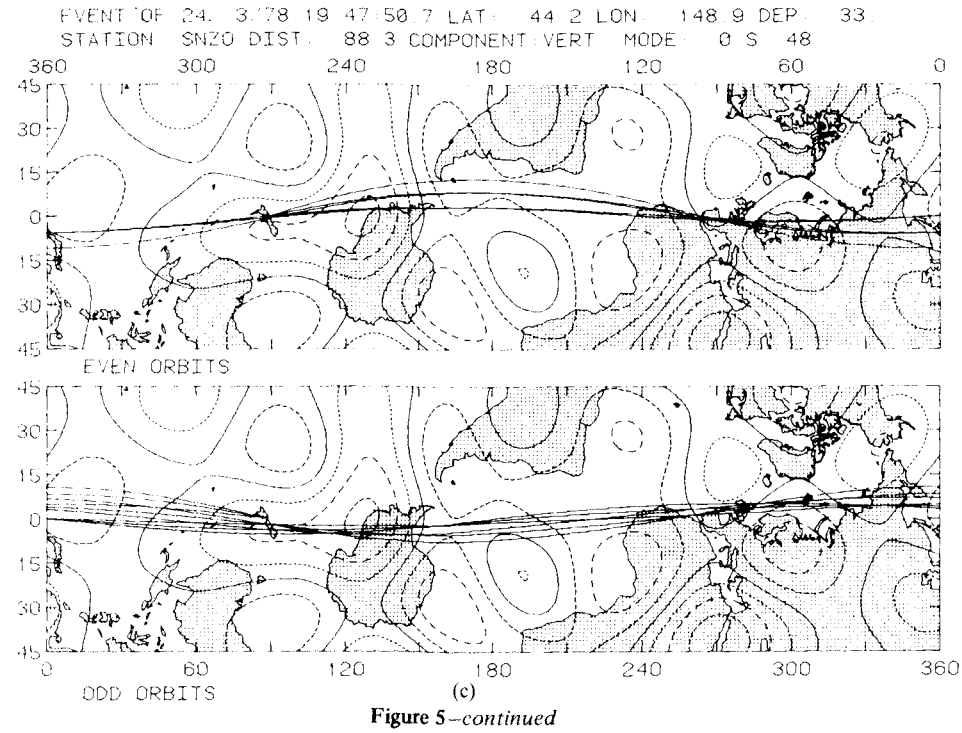

Figure 5—*continued*

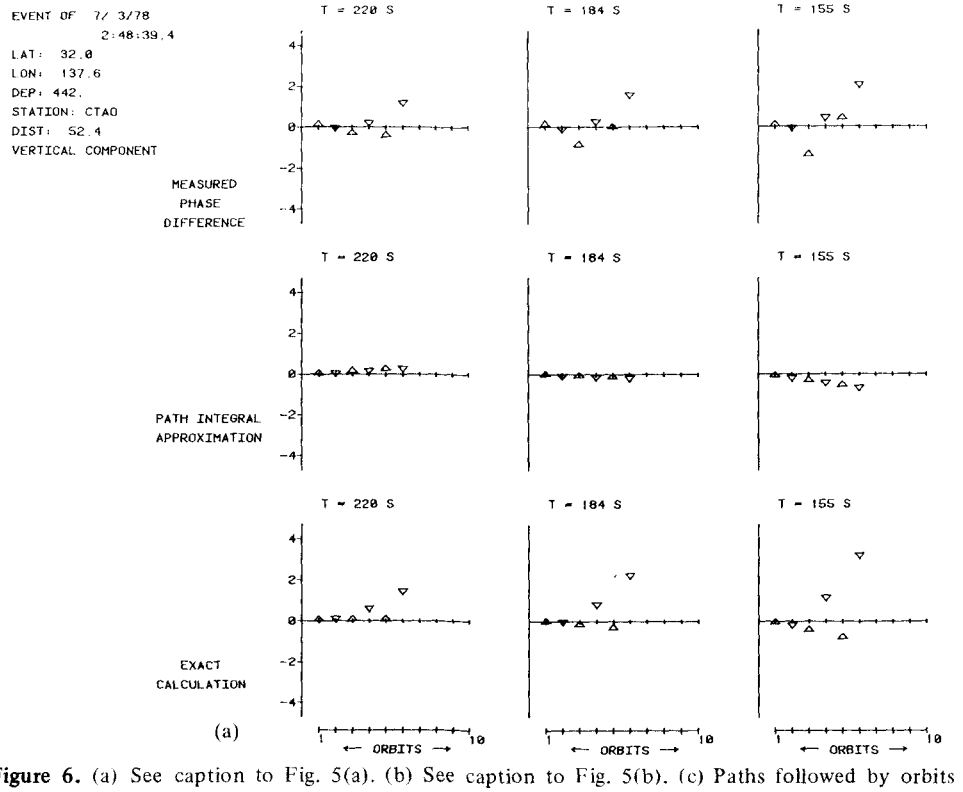

Figure 6. (a) See caption to Fig. 5(a). (b) See caption to Fig. 5(b). (c) Paths followed by orbits of Fig. 6(a, b).

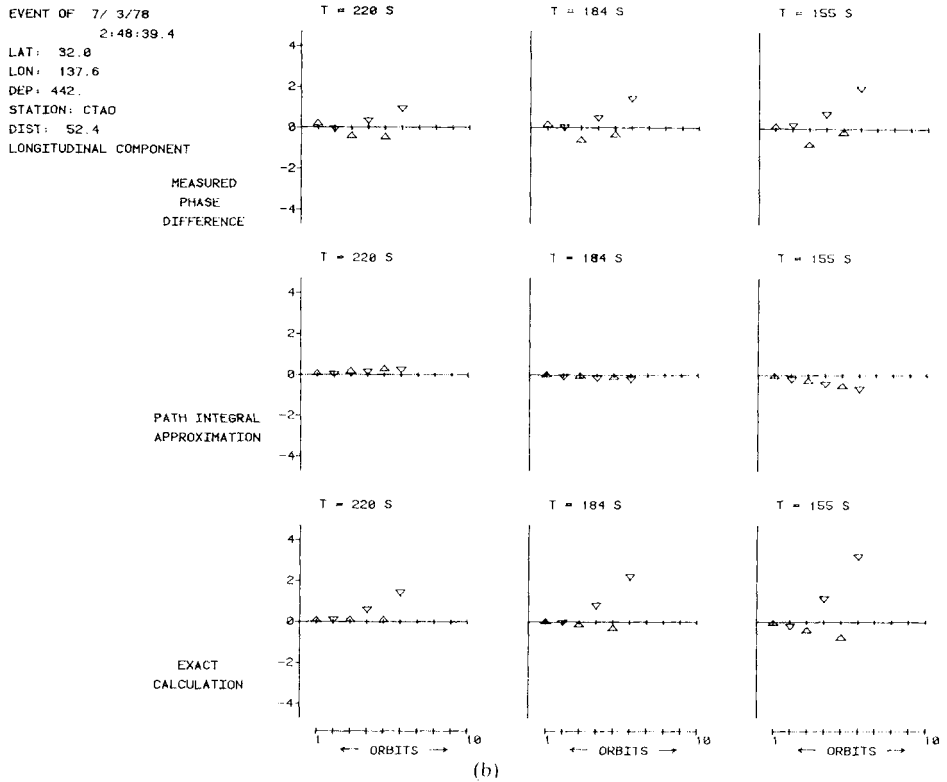

(b)

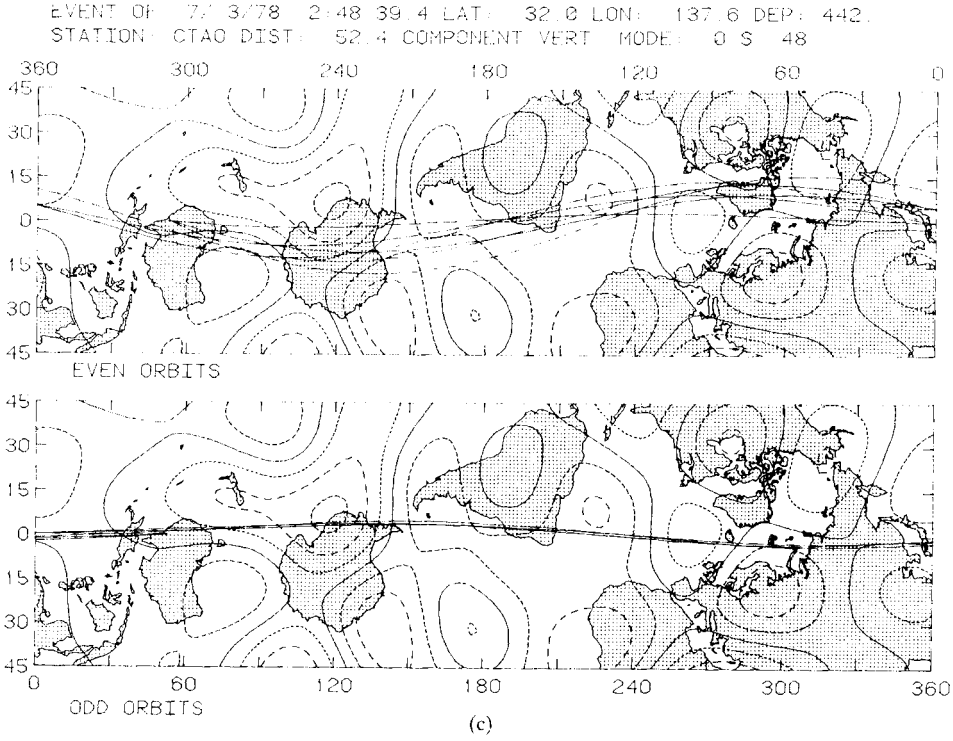

(c)

Figure 6–*continued*

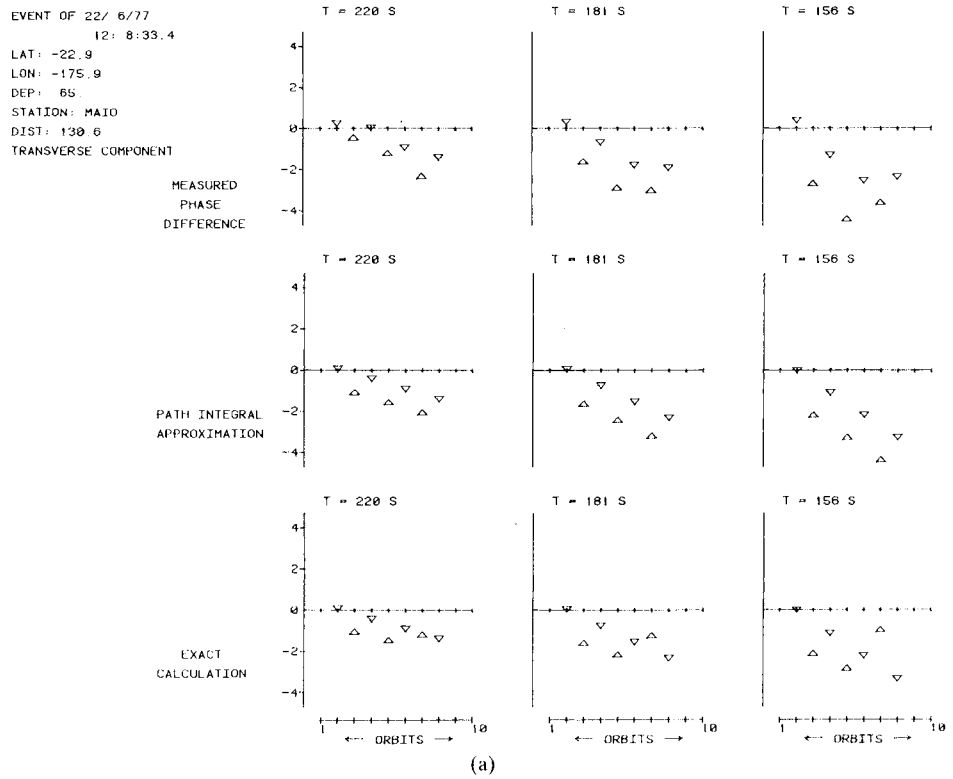

(a)

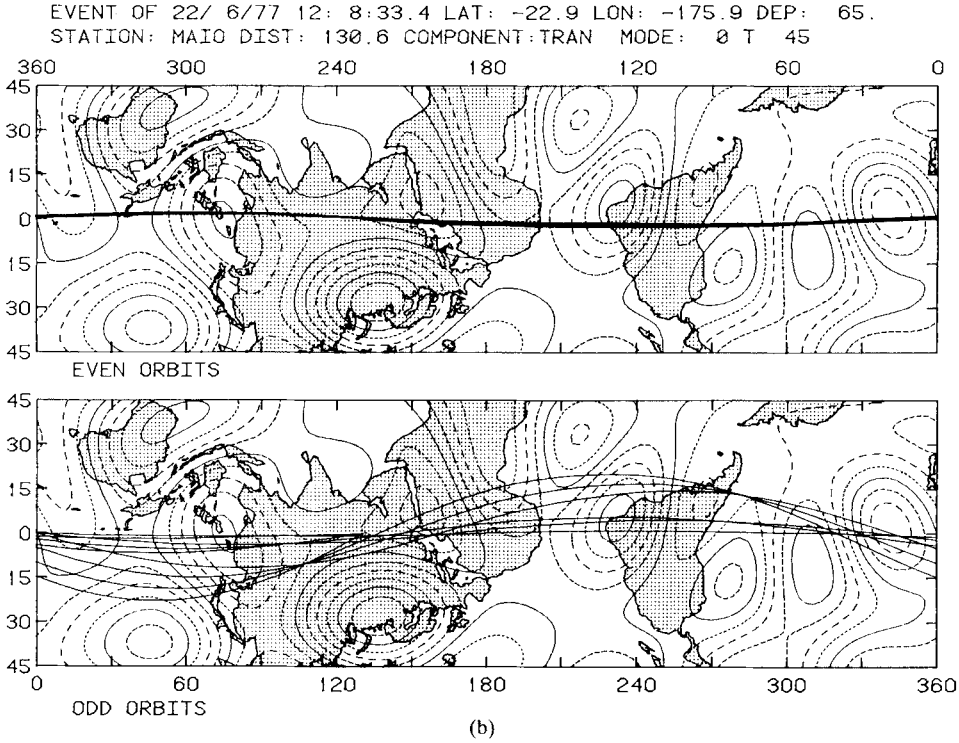

(b)

Figure 7. (a) See caption to Fig. 5(a); transverse component. (b) Paths followed by orbits of (a).

agreement with the theoretical predictions of the upper mantle model M84C of Woodhouse & Dziewonski (1984). These are of particular interest since one has some degree of confidence that the ray paths calculated for the model are also realistic. For phase we find that in general the path integral approximation is adequate for the first four or five orbits and that it is much better for Rayleigh waves than for Love waves at the same period. High orbit Love waves, at 150–200 s period, often show large and obvious phase anomalies that are far from the path integral approximation. It is, perhaps, surprising that the qualitative agreement of the amplitude data with the model is as good as it is, since we have shown that amplitudes are sensitive to second derivatives of phase velocity. We would conclude, therefore, that a significant fraction of the power in the second derivative of phase velocity is contained in degrees less than 8 – the degree to which the model is expanded. It is true, however, that in general the model significantly underpredicts amplitude anomalies. The model correctly predicts whether odd orbits are amplified or deamplified relative to even orbits approximately 75 per cent of the time.

In Fig. 3(a) we show measured Rayleigh wave amplitude anomalies at three periods (top row) for the vertical component record at NWAO. The measurements were made by deriving the least-squares filter which most accurately transforms a synthetic trace for each orbit into the observed trace. The values plotted for amplitude and phase are then evaluated using the filter coefficients. In calculating the synthetic traces, we employ the spherically symmetric attenuation of PREM (Dziewonski & Anderson 1981). The middle row of Fig. 3a, and later figures, shows the theoretical predictions based upon the path integral approximations derived above (Equations 53, 54) and the model M84C; the bottom row shows the theoretical results obtained by exact ray tracing. In Fig. 3a the data clearly show the opposite linear trend for even orbits (down triangles) and odd orbits (up triangles), as predicted by (54). The agreement with the model calculations is fairly good, but the exact calculations show significant nonlinearity – i.e. deviation from (54). Fig. 3b shows the paths corresponding to the orbits of Fig. 3a (at 184 s period) in a projection such that the source is on the 'equator' at the left side of the plot. The receiver is also on the 'equator', and thus the great circle path is a straight line through the centre of the map. The paths in this case do not show very large deviations from the great circle.

Fig. 4a shows results for Love waves, using a transverse component record at BCAO. This is a case in which both the data and the ray-tracing calculations show substantial deviations from the path integral approximation. This is diagnostic of substantial path deviations, and in Fig. 4b we see that paths deviate from the great circle by more than 15°. Fig. 5 shows an example of phase measurements for which Fermat's principle (middle row) is totally inapplicable. Measurements have been made independently from the vertical component (Fig. 5a) and the longitudinal component (Fig. 5b) at the same station. Both the data and the exact ray tracing calculations show that the great circle path appears to be fast for even orbits and slow for odd orbits. It should be borne in mind that the late orbits are subject to contamination by noise, since the amplitudes are small. The paths are shown in Fig. 5c. It can be seen that the odd orbits travel through slow regions SE of New Zealand, W of South Africa and in the Bering Sea that are largely avoided by the even orbits. The even orbits, on the other hand, pass more centrally through the high velocity region of the Baltic–Siberian shield. Fig. 6(a, b) shows Rayleigh wave phase measurements for another highly anomalous path. In this case the path deviations are large for even orbits, whereas odd orbits are not greatly deviated. Fig. 7a shows an example for Love waves, in which orbits G_2–G_6 show good agreement with the path integral approximation. G_7 is highly anomalous in the model calculation, deviating from the great circle by nearly 25°. The data also show erratic behaviour, but are not in agreement with the model.

Discussion

The character of amplitude and phase variations in mantle waves has been shown to be diagnostic of substantial lateral refraction. Sometimes this is so large that the great circle path can appear to be slow for orbits of one sense and fast for those of the opposite sense. There is a tendency for even and odd orbit paths to polarize and thus to sample somewhat different areas of the globe. Amplitude anomalies are predicted to have systematic and opposite trends for even and odd orbits and this is very commonly observed in the data. The slope of these trends is sensitive to the great circle integral of the second transverse derivative of phase velocity, with a range dependent kernel which also depends upon epicentral distance.

A technique has been formulated for calculating the functional derivatives of amplitude and phase with respect to global variations in phase velocity. Amplitude measurements, interpreted through ray theory, constitute a new source of information on global heterogeneity which potentially has higher resolution than phase measurements. The existence of large deviations in paths should also enhance the resolution of the phase data since it provides the opportunity of obtaining independent information from successive orbits in the same seismogram, and of reducing one source of error in the current methods of analysis.

In this paper, we have not addressed the possibility of multipathing; we assume that the first ray that is found, using the shooting method, is the only ray contributing to the seismogram. In general this will be the ray which, at the source, is closest in azimuth to the azimuth of the great circle path. The fact that the data show good agreement with the qualitative predictions of the theory suggests that multipathing is not an important phenomenon for mantle waves in the period range of this study but it certainly cannot be ruled out.

The question has been raised by a reviewer, and also in conversations with colleagues, that, since ray paths are minimum travel time paths for phase velocity, the path integral approximation will always give a value of phase anomaly which is greater than the true value and consequently phase velocity models based upon Fermat's principle will be biased. In Fig. 5(a, b), however, it may be noted that the difference between the path integral approximation for phase anomaly (middle panels) and the result obtained by exact ray tracing (bottom panels) is not uniformly of the same sign. The reason for this is that while the ray is a *stationary* path for phase travel time, it is a *minimum* time path only for the minor arc arrival (R_1 or G_1). For subsequent orbits the ray is neither a minimum nor a maximum time path. This is most easily demonstrated in the case of a spherically symmetric earth, for which the discussion may be limited to path length. It is, of course, well known that the minor arc great circle connecting two points on a sphere is of minimum length. However, consider now, any path containing a major arc great circle segment ABC where A and C are the endpoints of the arc and B is the midpoint. It is clear that any perturbation of the minor arc AB, keeping A and B (and BC) fixed, will yield a longer path. On the other hand, if B′ is a point close to B, not lying on ABC and if AB′ and B′C are great circle minor arcs, then the path AB′C is shorter than ABC. Consequently ABC has neither maximum nor minimum length.

A phase velocity model based upon minor arc orbits R_1, G_1 will, therefore, be biased, but by a very small amount since deviations from Fermat's principle are small for these orbits. For models based upon higher orbits, the question of the existence and sign of the bias due to the effects of lateral refraction can be answered only with reference to the particular suite of observations used, and the answer will also depend upon the Earth's true phase velocity distribution.

Acknowledgments

We thank Jon Peterson, John Hoffman and the staff of the Albuquerque Seismological Laboratory and John Berger and Duncan Agnew of the IDA project for providing digital seismic data. We also thank the anonymous reviewers for their helpful comments and suggestions. This research was carried out with the support of National Science Foundation under the grants EAR83-13330 and EAR85-11400.

References

Backus, G. E., 1964. Geographical interpretation of measurements of average phase velocities of surface waves over great circular and great semi-circular paths, *Bull. seism. Soc. Am.*, **54,** 571–610.

Dziewonski, A. M., 1971. On regional differences in dispersion of mantle Rayleigh waves, *Geophys. J. R. astr. Soc.*, **22,** 289–325.

Dziewonski, A. M. & Anderson, D. L., 1981. Preliminary reference earth model (PREM), *Phys. Earth. planet Int.*, **25,** 297–356.

Dziewonski, A. M. & Steim, J. M., 1982. Dispersion and attenuation of mantle waves from waveform inversion, *Geophys. J. R. astr. Soc.*, **70,** 503–527.

Goldstein, H., 1959. *Classical Mechanics,* Addison-Wesley, 399 pp.

Jobert, N. & Jobert, G., 1983. An application of ray theory to the propagation of waves along a laterally heterogeneous spherical surface, *Geophys. Res. Lett.*, **10,** 1148–1151.

Julian, B. R. & Gubbins, D., 1977. Three dimensional seismic ray tracing, *J. geophys. Res.*, **43,** 95–113.

Kanamori, H., 1970. Velocity and Q of mantle waves, *Phys. Earth planet. Int.*, **2,** 259–275.

Lay, T. & Kanamori, H., 1985. Geometric effects of global lateral heterogeneity on long period surface wave propagation, *J. geophys. Res.*, **90,** 605–621.

Mills, J. M., 1978. Great circle Rayleigh wave attenuation and group velocity, Part IV: Regionalization and pure-path models for shear velocity and attenuation, *Phys. Earth planet. Int.*, **17,** 323–352.

Nakanishi, I. & Anderson, D. L., 1982. Worldwide distribution of group velocity of mantle waves as determined by spherical harmonic inversion, *Bull. seism. Soc. Am.*, **72,** 1185–1194.

Nakanishi, I. & Anderson, D. L., 1983. Measurements of mantle wave velocities and inversion for lateral heterogeneity and anisotropy, Part I. Analysis of great circle phase velocities, *J. geophys. Res.*, **88,** 10267–10283.

Richards, P. G., 1971. An elasticity theorem for heterogeneous media, with an example of body wave dispersion in the Earth, *Geophys. J. R. astr. Soc.*, **22,** 453–472.

Thomson, C., 1983. Ray-theoretical amplitude inversion for laterally varying velocity structure below NORSAR, *Geophys. J. R. astr. Soc.*, **74,** 525–558.

Toksöz, M. N. & Anderson, D. L., 1966. Phase velocities of long-period surface waves and structure of the upper mantle 1, Great circle Love and Rayleigh wave data, *J. geophys. Res.*, **71,** 1649–1658.

Wong, Y. K. & Woodhouse, J. H., 1983. Ray theory for surface waves on a sphere, *EOS,* **64,** 260.

Wong, Y. K. & Woodhouse, J. H., 1984. Amplitude, phase and path anomalies for mantle waves, *EOS,* **65,** p. 244.

Woodhouse, J. H., 1974. Surface waves in a laterally varying layered structure, *Geophys. J. R. astr. Soc.*, **37,** 461–490.

Woodhouse, J. H. & Dziewonski, A. M., 1984. Mapping the upper mantle: Three dimensional modeling of earth structure by inversion of seismic waveforms, *J. geophys. Res.*, **89,** 5953–5986.